Hindawi
Mathematical Problems in Engineering
Volume 2020, Article ID 3584048, 11 pages
https://doi.org/10.1155/2020/3584048

Research Article

Vibrational Energy Flow Model for a High Damping Beam with Constant Axial Force

Xiaoyan Teng,[1] Nan Liu,[1] and Jiang Xudong[2]

[1]*School of Mechanical and Electrical Engineering, Harbin Engineering University, Harbin 150001, China*
[2]*School of Mechanical and Power Engineering, Harbin University of Science and Technology, Harbin 150080, China*

Correspondence should be addressed to Jiang Xudong; xudongjiang@sina.com

Received 4 January 2020; Revised 27 May 2020; Accepted 22 June 2020; Published 17 July 2020

Academic Editor: Ivano Benedetti

The energy flow analysis (EFA) method is developed to predict the energy density of a high damping beam with constant axial force in the high-frequency range. The energy density and intensity of the beam are associated with high structural damping loss factor and axial force and introduced to derive the energy transmission equation. For high damping situation, the energy loss equation is derived by considering the relationship between potential energy and total energy. Then, the energy density governing equation is obtained. Finally, the feasibility of the EFA approach is validated by comparing the EFA results with the modal solutions for various frequencies and structural damping loss factors. The effects of structural damping loss factor and axial force on the energy density distribution are also discussed in detail.

1. Introduction

With the development of high-speed aircrafts and transportation vehicles, high-frequency vibration of components is of great concern for both academic and industrial communities in recent years. As one of the typical structural components, beams with high damping treatment for vibrational reduction are extensively used in mechanical and aerospace engineering. Moreover, these beam-type structures sometimes experience axial forces arising from initial stress and temperature variation, which can significantly influence the dynamic characteristics of structures. Consequently, high-frequency dynamic response prediction of a high damping beam with axial force is of great significance for a beam-type structure design.

Both the statistical energy analysis (SEA) [1] and the energy flow analysis (EFA) [2] are popular methods to predict structural time and space averaged energy densities in high-frequency range. SEA only can provide a single averaged energy value for each subsystem of a built-up structure. As an alternative method to SEA, EFA can provide the locally smoothed energy value at every interested point in a built-up structure. As a consequence, EFA is more advantageous over SEA in solving high-frequency dynamic responses due to its ability to obtain detailed local response information.

Wohlever et al. [3] derived the energy density governing equation of hysterically damped rods and beams from traditional displacement solutions. Chen et al. [4] calculated the transient response of beams under high-frequency shock load by energy finite element method and virtual mode synthesis method. Liu et al. [5] developed the vibrational energy flow model for functionally graded beams for high-frequency response prediction. Kong et al. [6] theoretically tested the validity region and criterion of EFA from the formation of reverberant plane wave field. Nokhbatolfoghahai et al. [7] and Navazi et al. [8] verified the vibrational energy flow model of a uniform beam and plate from experimental data. Zhu et al. [9] developed a hybrid method for midfrequency vibrational problems, which combined FEA for the stiff member and EFA for the reverberant field of the flexible member. Sadeghmanesh et al. [10] presented a method for defining a criterion to select a proper structural theory based on the order of shear deformation and rotary inertia for low- to high-frequency vibration analyses. Furthermore, the influences of the fluid loading on the dynamic

behaviors of structures were considered such that EFA was applied to model the interaction of the fluid with structures [11–13]. There usually exist the discontinuities, which refer to material and structural configuration variation for the coupled structures in engineering. The energy density is not continuous on coupling boundaries where wave reflection and transmission arise from encountering the discontinuities. In the conventional EFA coupling approach, FEM is used to solve the energy density governing equation and the wave-based method is utilized to obtain the power transferring coefficients [14–16]. Park and Hong [17] and Zhihui et al. [18] developed a hybrid power flow analysis method using coupling loss factor of SEA to solve the coupling problems in EFA. Kwon et al. [19] and Zheng et al. [20] developed an energy flow model for high-frequency vibroacoustic analysis of complex structures using EFA method.

For structures with initial stress, Zhang et al. [21] and Di et al. [22] investigated the effects of the axial force due to thermal expansion on the high-frequency vibration of beams and plates. Recently Zhang et al. [23] have derived the energy density governing equation by considering the energy density and intensity associated with axial force, which is neglected in [21, 22]. Unfortunately the developed EFA can only be used to analyze the high-frequency vibration of lightly damping beams. In this paper, we extend the EFA model developed by Zhang et al. [23] to high damping beams with axial force. This paper is organized as follows. Firstly, the energy density governing equation is derived from the energy transmission equation and the energy loss equation for a high damping beam with axial force. Particularly, the relationship between energy density and intensity of structures and the dissipated energy equation are derived from the wavenumber obtained without approximation of the real and imaginary term. Then the accuracy of the presented formulation is verified by comparing the developed EFA results with modal analysis results of a pinned-pinned beam with high damping loss factor and axial force. The effects of damping loss factor and axial force on the energy density distribution are also discussed. Finally, the present EFA method is applied to beams with different boundary conditions and conclusions on the new EFA model are given.

2. Energy Density Governing Equation of a High Damping Beam with Constant Axial Force

2.1. Energy Transmission Equation. For a beam with constant axial force, driven by a harmonic point force as depicted in Figure 1, the flexible motion equation can derived as [24, 25]

$$D_c\frac{\partial^4 w}{\partial x^4} - N_c\frac{\partial^2 w}{\partial x^2} + \rho S\frac{\partial^2 w}{\partial t^2} = F_0 e^{j\omega t}\delta(x - x_0), \quad (1)$$

where w is the transverse displacement of the vibrating beam, $D_c = D(1 + j\eta)$ is the complex bending stiffness with D representing the real part of D_c and η the structural damping loss factor, $N_c = N(1 + j\eta)$ is the complex axial load with N representing the real constant part of N_c, ρ is the mass density, S is the cross-section area, $F_0 e^{j\omega t}\delta(x - x_0)$ is the transverse harmonic load applied at point x_0 with F_0 denoting its amplitude, and ω is its circular frequency, $\delta(x - x_0)$ is the Delta function, L is the length of the beam.

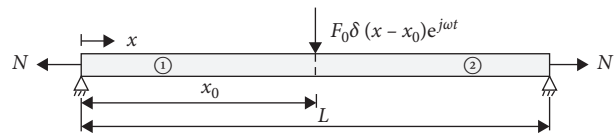

Figure 1: A pined-pinned transversely vibrating beam with constant axial force.

Substituting the general solution $w(x,t) = Ce^{j(kx+\omega t)}$ into equation (1) gives the dispersion relation:

$$D_c k^4 + N_c k^2 - \rho S\omega^2 = 0. \quad (2)$$

Then the complex wavenumber, k, can be solved from equation (2) and be presented as

$$\begin{cases} k = \pm k_{c1},\ \pm jk_{c2}, \\ k_{c1} = \sqrt{\dfrac{-N_c}{2D_c} + \sqrt{\left(\dfrac{N_c}{2D_c}\right)^2 + \left(\dfrac{\rho S\omega^2}{D_c}\right)}}, \\ k_{c2} = \sqrt{\left(\dfrac{N_c}{2D_c}\right) + \sqrt{\left(\left(\dfrac{N_c}{2D_c}\right)\right)^2 + \left(\dfrac{\rho S\omega^2}{D_c}\right)}}, \end{cases} \quad (3)$$

where $k_{c1} = k_1 + jk_2$ is the complex wavenumber, k_1 and k_2 are the corresponding real and imaginary parts, respectively.

In terms of equation (2), the group velocity c_g can be expressed as equation (4) by implicit derivative with respect to the real part k_1 of the complex wavenumber k_{c1}:

$$c_g = \frac{\partial\omega}{\partial k_1} = \frac{D(2k_1^3 - 6k_1k_2^2 - 6\eta k_1^2k_2 + 2\eta k_2^3) + N(k_1 - \eta k_2)}{\rho S\omega}. \quad (4)$$

In a lightly damped system, from equations (3) and (4), the higher-order terms with respect to the structural damping can be neglected and the flexural wavenumber and group velocity can be approximated as [21, 23]

$$k_1 \approx \sqrt{-\frac{N}{2D} + \sqrt{\left(\frac{N}{2D}\right)^2 + \frac{\rho S\omega^2}{D}}}, \quad (5)$$

$$k_2 \approx -\eta\frac{\rho S\omega^2}{4Dk_1^3 + 2Nk_1},$$

$$c_g \approx \frac{2Dk_1^3 + Nk_1}{\rho S\omega}. \quad (6)$$

As a result, the general solution of equation (1) is expressed as

$$w(x,t) = \left(Ae^{-jk_{c1}x} + Be^{jk_{c1}x} + Ge^{-k_{c2}x} + He^{k_{c2}x}\right)e^{j\omega t}, \quad (7)$$

where A, B, G, and H are complex coefficients that can be calculated from the boundary conditions.

The right first two terms of equation (7) are far-field solutions representing the propagating wave, while the right last two ones of equation (7) are near-field solutions representing the evanescent wave. For high-frequency vibration, the flexible wavelength is quite short. The near-field solutions are neglected beyond one wavelength away from the boundaries and driving points where they are dissipated rapidly. Thus, only the far-field solutions are taken into account for EFA and the expression of displacement is rewritten as

$$w(x,t) = \left(Ae^{-jk_{c1}x} + Be^{jk_{c1}x}\right)e^{j\omega t}. \tag{8}$$

The energy density in a vibrating beam is the sum of the kinetic and potential energy densities which are associated with bending strain and constant axial force, respectively. The time averaged energy density can be represented as [3, 26]

$$\langle e\rangle = \frac{1}{4}\mathrm{Re}\left[\rho S\left(\frac{\partial w}{\partial t}\right)\left(\frac{\partial w}{\partial t}\right)^{*} + D_c\left(\frac{\partial^2 w}{\partial x^2}\right)\left(\frac{\partial^2 w}{\partial x^2}\right)^{*} + N_c\left(\frac{\partial w}{\partial x}\right)\left(\frac{\partial w}{\partial x}\right)^{*}\right], \tag{9}$$

where the bracket operator $\langle\cdot\rangle$ denotes the time average over one period and the superscript $*$ denotes the complex conjugate operator. The total intensity is associated with the shear force, the bending moment, and the constant axial force. The time averaged intensity of the vibrating beam is presented as [3, 26]

$$\langle I\rangle = \frac{1}{2}\mathrm{Re}\left[D_c\left(\frac{\partial^3 w}{\partial x^3}\right)\left(\frac{\partial w}{\partial t}\right)^{*} - D_c\left(\frac{\partial^2 w}{\partial x^2}\right)\left(\frac{\partial^2 w}{\partial x\,\partial t}\right)^{*} - N_c\left(\frac{\partial w}{\partial x}\right)\left(\frac{\partial w}{\partial t}\right)^{*}\right]. \tag{10}$$

Substituting equation (8) into equations (9) and (10), and space averaging over a wavelength, the time and space averaged energy density and intensity can be obtained as

$$\overline{\langle e\rangle} = \frac{1}{4}\left(\rho S\omega^2 + N\left|k_{c1}\right|^2 + D\left|k_{c1}\right|^4\right)\left(\alpha_1|A|^2e^{2k_2x} + \alpha_2|B|^2e^{-2k_2x}\right), \tag{11}$$

$$\overline{\langle I\rangle} = \frac{1}{2}\omega\mathrm{Re}\left[D_ck_{c1}^3 + D_ck_{c1}\left|k_{c1}\right|^2 + N_ck_{c1}\right]\left(\alpha_1|A|^2e^{2k_2x} - \alpha_2|B|^2e^{-2k_2x}\right), \tag{12}$$

where $\overline{\langle\cdot\rangle}$ denotes the time and space averaged operator to eliminate the spatially harmonic terms, α_1 and α_2 are the space averaging values of e^{2k_2x} and e^{-2k_2x}.

From equations (11) and (12), the relationship between the time and space averaged energy density and intensity, so-called energy transmission equation, is derived as

$$\overline{\langle \mathrm{I}\rangle} = \frac{\omega\mathrm{Re}\left[D_ck_{c1}^3 + D_ck_{c1}\left|k_{c1}\right|^2 + N_ck_{c1}\right]}{k_2\left(\rho S\omega^2 + N\left|k_{c1}\right|^2 + D\left|k_{c1}\right|^4\right)}\frac{\mathrm{d}\overline{\langle e\rangle}}{\mathrm{d}x}. \tag{13}$$

2.2. Energy Loss Equation. In the case of hysteric damping, the dissipated power of per volume smoothed by time and space averaging is proportional to the potential energy density smoothed by time and space averaging, for an elastic system harmonically vibrating with frequency ω

$$\overline{\langle \pi_{\mathrm{diss}}\rangle} = 2\eta\omega\overline{\langle e_p\rangle}, \tag{14}$$

where e_{p} is the potential energy density. In a lightly damped system, the potential energy density is equal to the kinetic energy, and hence the dissipated power is expressed as $\overline{\langle \pi_{\mathrm{diss}}\rangle} = \eta\omega\overline{\langle e\rangle}$.

In a vibrating beam with constant axial force, the time averaged potential energy density can be expressed as [27]

$$\langle e_p\rangle = \frac{1}{4}\mathrm{Re}\left[D_c\left(\frac{\partial^2 w}{\partial x^2}\right)\left(\frac{\partial^2 w}{\partial x^2}\right)^{*} + N_c\left(\frac{\partial w}{\partial x}\right)\left(\frac{\partial w}{\partial x}\right)^{*}\right]. \tag{15}$$

Substituting equation (8) into equation (15) and smoothed by local space averaging, equation (15) can be rewritten as

$$\overline{\langle e_p\rangle} = \frac{1}{4}\left(D\left|k_{c1}\right|^4 + N\left|k_{c1}\right|^2\right)\left(\alpha_1|A|^2e^{2k_2x} + \alpha_2|B|^2e^{-2k_2x}\right). \tag{16}$$

Combining equations (11), (14), and (16), the relationship between time and locally space averaged energy density and the dissipated power of per volume can be represented as

$$\overline{\langle \pi_{\mathrm{diss}}\rangle} = \frac{2\eta\omega\left(N\left|k_{c1}\right|^2 + D\left|k_{c1}\right|^4\right)}{\rho S\omega^2 + N\left|k_{c1}\right|^2 + D\left|k_{c1}\right|^4}\overline{\langle e\rangle}. \tag{17}$$

2.3. Energy Density Governing Equation. For the elastic medium, the power balance equation at the steady state is expressed as

$$\frac{d\overline{\langle I\rangle}}{dx}+\overline{\langle \pi_{\mathrm{diss}}\rangle}=\overline{\langle \pi_{\mathrm{in}}\rangle}\delta(x-x_0), \tag{18}$$

where π_{in} refers to the input power at the driving point $x = x_0$.

Substituting equations (13) and (17) into equation (18), the energy density governing equation for the high damping beam with axial force can be derived as

$$\frac{\omega\mathrm{Re}\left[D_c k_{c1}^3+D_c k_{c1}\left|k_{c1}\right|^2+N_c k_{c1}\right]}{k_2\left(\rho S\omega^2+N\left|k_{c1}\right|^2+D\left|k_{c1}\right|^4\right)}\frac{\mathrm{d}^2\overline{\langle e\rangle}}{\mathrm{d}x^2}+\frac{2\eta\omega\left(N\left|k_{c1}\right|^2+D\left|k_{c1}\right|^4\right)}{\rho S\omega^2+N\left|k_{c1}\right|^2+D\left|k_{c1}\right|^4}\overline{\langle e\rangle}=\overline{\langle \pi_{\mathrm{in}}\rangle}\delta(x-x_0). \tag{19}$$

Unlike the lightly damping system in [23], the energy transition equation is derived using the exact wavenumber without neglecting higher-order damping terms. The energy transition equation represents the relationship between time and space averaged energy density and intensity without group velocity because the damping effect is not neglected. On account of high structural damping, the potential energy density is not the same as the kinetic energy density of the structure. Thus, the energy loss equation is derived according to the relationship between potential energy and total energy.

3. Solution of Energy Density Governing Equation

As shown in Figure 1, the beam is divided into two regions at x_0. From equation (19), the general solution of the flexural energy density governing equation is expressed as

$$\overline{\langle e_f\rangle}_i=C_{i1}\mathrm{e}^{-\lambda_f x}+C_{i2}\mathrm{e}^{\lambda_f x},\quad (i=1,2), \tag{20}$$

$$\lambda_f=\sqrt{-\frac{2\eta k_2\left(N\left|k_{c1}\right|^2+D\left|k_{c1}\right|^4\right)}{\mathrm{Re}\left[D_c k_{c1}^3+D_c k_{c1}\left|k_{c1}\right|^2+N_c k_{c1}\right]}}, \tag{21}$$

where the subscript i denotes the i^{th} region of the beam. The constants C_{i1}, C_{i2} can be determined by the energy boundary conditions.

From equations (13) and (20), the energy intensity of the vibrating beam is represented as

$$\overline{\langle I_f\rangle}_i=P_f\left(C_{i1}e^{-\lambda_f x}-C_{i2}e^{\lambda_f x}\right), \tag{22}$$

$$P_f=-\lambda_f\frac{\omega\mathrm{Re}\left[D_c k_{c1}^3+D_c k_{c1}\left|k_{c1}\right|^2+N_c k_{c1}\right]}{k_2\left(\rho S\omega^2+N\left|k_{c1}\right|^2+D\left|k_{c1}\right|^4\right)}. \tag{23}$$

Because there are no energy outflow and inflow at both ends of the pinned-pinned beam, the following energy intensity boundary conditions can be determined as

$$\overline{\langle I_f\rangle}_1(0)=0,\ \overline{\langle I_f\rangle}_2(L)=0. \tag{24}$$

At the interface between the regions ① and ②, the energy density is continuous and the energy intensity is subject to conservation of energy. The resulting boundary condition can be written as

$$\overline{\langle e_f\rangle}_1(x_0)=\overline{\langle e_f\rangle}_2(x_0), \tag{25}$$

$$\overline{\langle I_f\rangle}_2(x_0)=\overline{\langle I_f\rangle}_1(x_0)+\overline{\langle \pi_{\mathrm{in}}\rangle}. \tag{26}$$

The input power of the vibrating beam is obtained by the impedance method and expressed as [23, 28]

$$\overline{\langle \pi_{\mathrm{in}}\rangle}=\frac{1}{2}\left|F_0\right|^2\mathrm{Re}\left(\frac{1}{Z}\right), \tag{27}$$

$$Z=\frac{2D_c k_{c1}k_{c2}^2}{\omega}\left(1+j\frac{k_{c1}}{k_{c2}}\right), \tag{28}$$

where Z is the impedance at the driving point of the vibrating beam with axial force.

Substituting equation (20) into equations (24)~(26), the matrix equation can be obtained as

$$\begin{bmatrix}1 & -1 & 0 & 0\\ 0 & 0 & e^{-\lambda_f L} & -e^{-\lambda_f L}\\ e^{-\lambda_f x_0} & e^{\lambda_f x_0} & -e^{-\lambda_f x_0} & -e^{\lambda_f x_0}\\ -P_f e^{-\lambda_f x_0} & P_f e^{\lambda_f x_0} & P_f e^{-\lambda_f x_0} & -P_f e^{\lambda_f x_0}\end{bmatrix}\begin{bmatrix}C_{11}\\ C_{12}\\ C_{21}\\ C_{22}\end{bmatrix}=\begin{bmatrix}0\\ 0\\ 0\\ \overline{\langle \pi_{\mathrm{in}}\rangle}\end{bmatrix}. \tag{29}$$

According to equation (29), the flexural energy density can be analytically calculated for the vibrating beam with high structural damping loss factor and constant axial force.

4. Verification and Discussion

To validate the proposed EFA formulation and investigate the effects of structural damping loss factor and axial force, various energy flow analyses are performed for a pinned-pinned beam at both ends shown in Figure 1. The results from analytical solutions of EFA governing equation are compared with exact modal solutions (Appendix A and Appendix B), which are defined as time averaged energy density obtained from the displacement solutions. For each modal analysis, the first 5000 modes are extracted to ensure the accuracy of the solution. In addition, the present vibrational energy flow method is applied to beams with different boundary conditions.

4.1. Model Verification. The beam is made of aluminum alloy with density $\rho = 2700\mathrm{kg/m}^3$ and elastic modulus $E = 70\,\mathrm{GPa}$, and its dimensions are $L = 3\mathrm{m}S = 2\times10^{-4}\mathrm{m}^2$, $I_{\mathrm{b}} = 2\times10^{-10}\mathrm{m}^4$. The structural damping loss factor η

ranges from 0.05 to 0.8 and the axial force N from 0 to 20 kN, respectively. The pinned-pinned beam, as shown in Figure 1 is excited by a transverse harmonic force located at $x_0 = L/2$.

Figure 2 shows the energy density distribution of pinned-pinned beams for the case with the axial force $N = 20$ kN, the amplitude of transverse harmonic force $F_0 = 1$ N, and the structural damping loss factor $\eta = 0.5$ when the analysis frequencies are 2, 4, 6, and 8 kHz. Except for that the developed EFA results differ near both ends of the beam, the developed EFA results is analogous to the modal analysis results because the evanescent wave is neglected in the energy flow models. Moreover, it can be observed that the difference of the EFA solution from the modal solution is smaller at higher frequencies, and hence the accuracy of the EFA model is improved at higher frequencies. The energy density distributions with different amplitudes of transverse harmonic force ($F_0 = 0.1$, 1, 10 kN), as shown in Figure 3, are calculated when the excitation frequency is $f = 6$ kHz. It is also found that the EFA solutions are smooth representing the overall trend of modal solutions and in good agreement with modal solutions except the vicinity of boundaries. In addition, the global variation of energy density increases with larger amplitudes of harmonic point force.

The exact energy density distribution obtained by modal analysis method oscillates spatially without space averaging. At high-frequency ranges, the variance of classical solutions is uniform resulting from short wavelength. Therefore, the developed EFA results, obtained with space averaging, are analogous to the classical solutions as the analysis frequency increases.

Figures 4 and 5 show the energy density distributions of pinned-pinned beams with $N = 20$ kN, $F_0 = 1$ N, and $f = 6$ kHz when the structural damping loss factor is $\eta = 0.05$ and 0.5, respectively. If the structural damping loss factor is small, the wavenumber and group velocity given in equations (3) and (4) in the developed energy flow model are well approximated by those in equations (5) and (6) in the traditional energy flow model. Hence, in a low damping beam the developed EFA solution is close to the traditional EFA solution. However, in a high damping beam, the developed EFA result represents the trend of exact solution from modal analysis, and the developed EFA result concurs more with the exact solution than the traditional EFA result because higher-order damping terms are no longer neglected.

4.2. Effects of Constant Axial Force. Figure 6 shows the energy density distributions of pinned-pinned beams with different axial forces $0\text{kN} \le N \le 20\text{kN}$, amplitude of transverse harmonic force $F_0 = 1$ N, and structural damping loss factor $\eta = 0.5$ when the analysis frequency is 6 kHz. The energy density varies more dramatically along x position with increasing axial force. The total energy can be calculated from integrating the energy density over the length of the beam. Figure 7 shows that the total energy is higher at larger axial force.

The effects of constant axial force can be explained by the input power and group velocity. Figures 8 and 9 show the input power and group velocity, respectively. It is observed

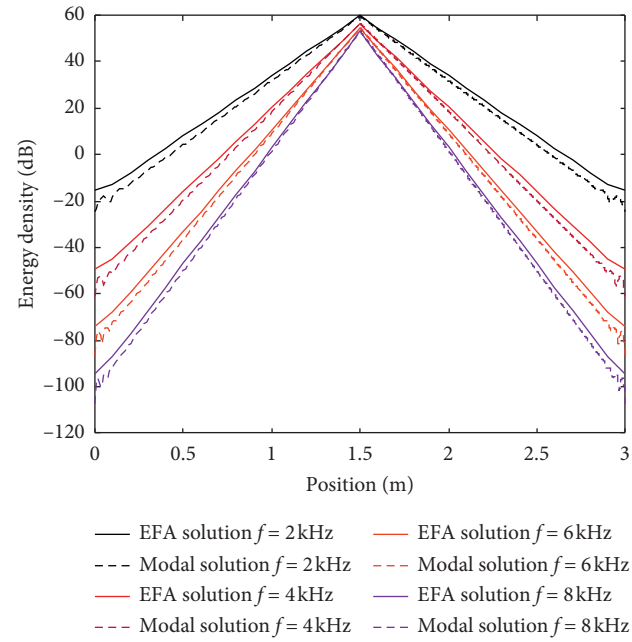

Figure 2: Energy density distribution of pinned-pinned beams with $N = 20$ kN, $F_0 = 1$ N, and $\eta = 0.5$ when $f = 2$, 4, 6, 8 kHz.

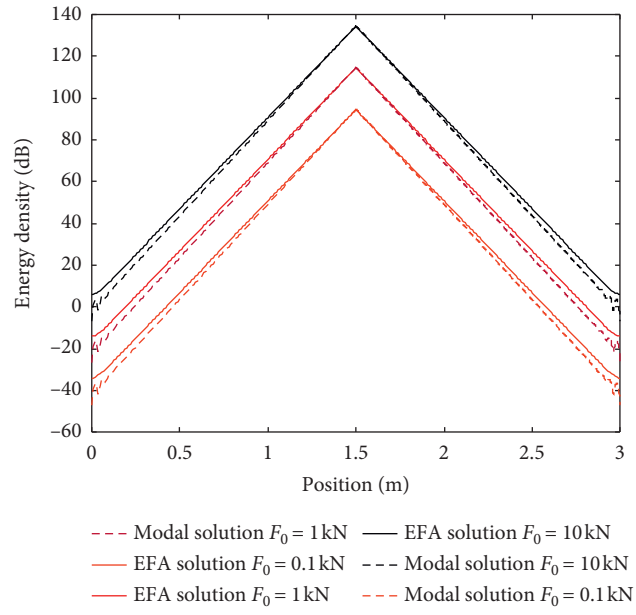

Figure 3: Energy density distribution of pinned-pinned beams with $N = 20$ kN, $\eta = 0.5$, and $f = 6$ kHz when $F_0 = 0.1$, 1, 10 kN.

that the input power increases and the group velocity decreases with increasing axial force. Because the total energy is proportional to the input power, the total energy is higher for larger axial force arousing larger input power. The lower group velocity makes energy propagate more slowly from the driving point to the boundary. It means that more energy dissipates near the driving point and less energy propagates to the boundary. As a result, the energy density changes more dramatically with larger axial force along the x position.

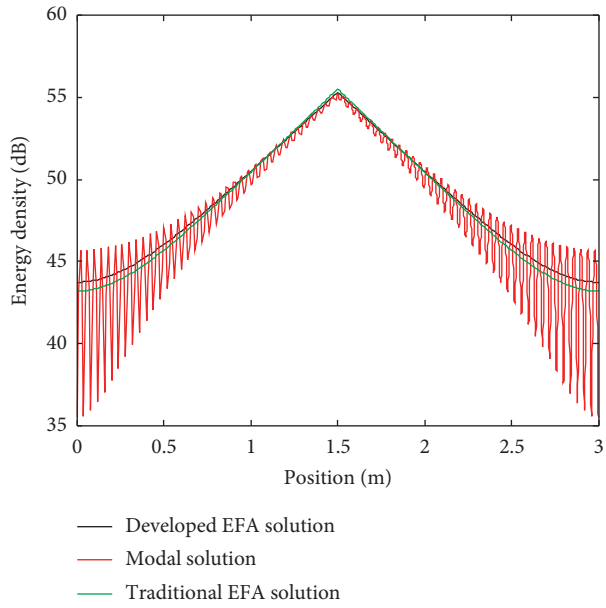

Figure 4: Energy density distribution of pinned-pinned beams with $N = 20$ kN, $F_0 = 1$ N, and $\eta = 0.05$ when $f = 6$ kHz.

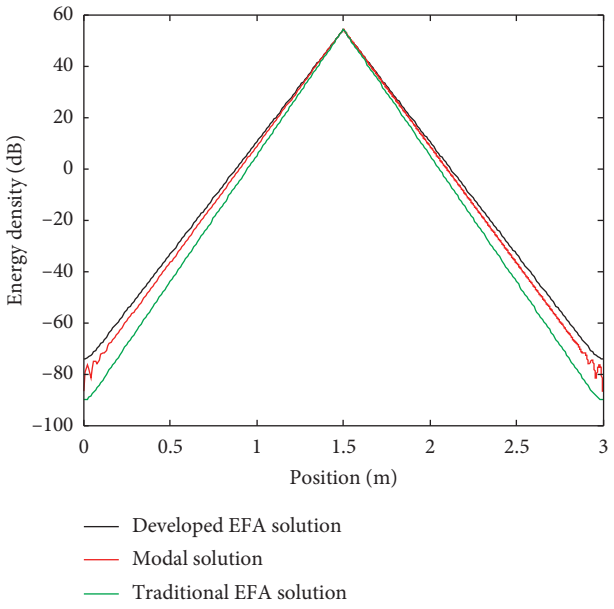

Figure 5: Energy density distribution of pinned-pinned beams with $N = 20$ kN, $F_0 = 1$ N, and $\eta = 0.05$ when $f = 6$ kHz.

4.3. Effects of Structural Damping Loss Factor. Figure 10 shows the energy density distributions of pinned-pinned beams with different structural damping loss factor $0 \le \eta \le 0.8$, amplitude of transverse harmonic force $F_0 = 1$ N, and axial force $N = 20$ kN when the analysis frequency is 6 kHz. The developed EFA results represent the global variation of the modal solutions at each structural damping loss factor. Owing to the exclusion of the evanescent wave, the developed energy flow solutions more closely approach the modal solutions as the structural damping loss factor increases. The energy density changes more suddenly along x position with increasing structural damping loss factor. Figure 11 shows that the total energy is lower at larger structural damping loss factor.

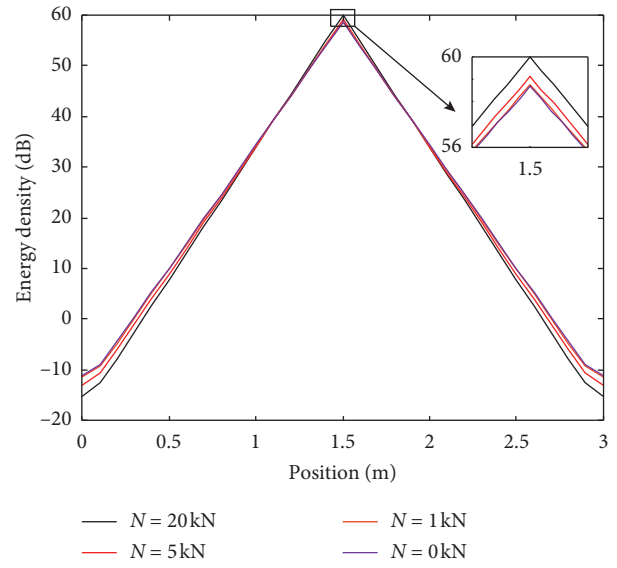

Figure 6: Energy density distribution of pinned-pinned beams with $f = 6$ kHz, $F_0 = 1$ N, and $\eta = 0.5$ when $N = 0$, 1, 5, 20 kN.

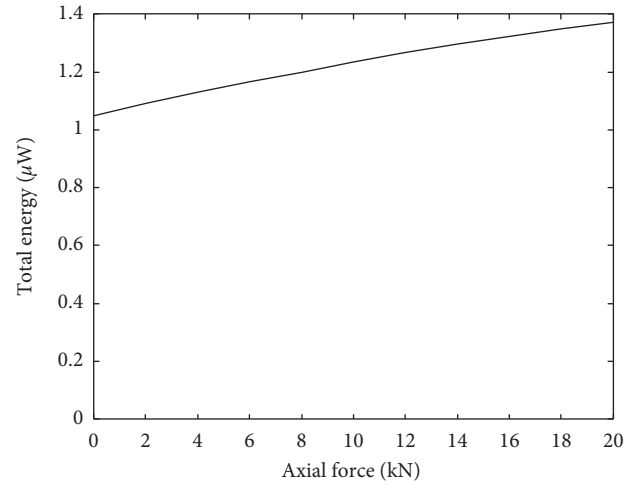

Figure 7: Total energy of pinned-pinned beams *versus* axial force with $F_0 = 1$ N, $\eta = 0.5$, and $f = 6$ kHz.

Figures 12 and 13 show the input power and group velocity at various structural damping loss factors, respectively. It is found that the input power decreases and the group velocity increases with an increase of structural damping loss factor. Since the total energy is proportional to the input power, the total energy is lower for larger structural damping loss factor leading to less input power. In fact, the larger group velocity contributes to flatter change of the energy density along the x position. But the energy density distribution changes more dramatically with larger structural damping loss factor along the x position. It attributes to that the energy density is mainly affected by the input power while the effect of group velocity is minor.

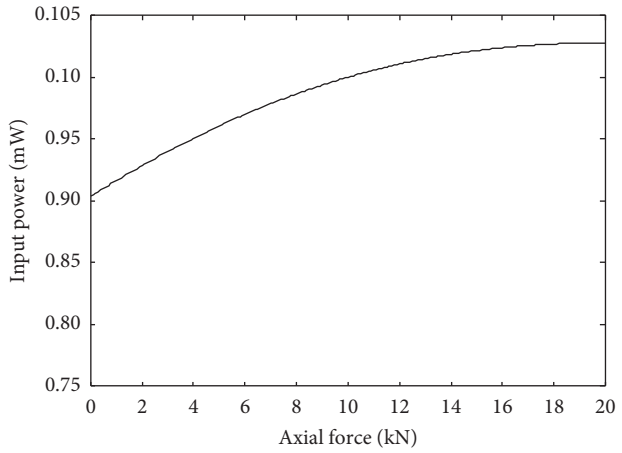

FIGURE 8: Input power of pinned-pinned beams *versus* axial force with $F_0 = 1$ N, $\eta = 0.5$ and $f = 6$ kHz.

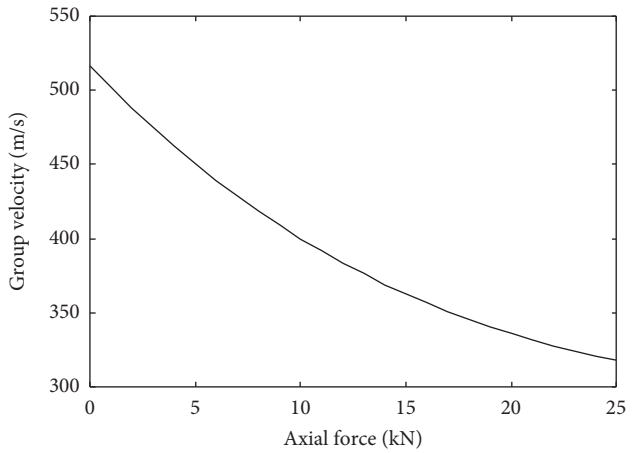

FIGURE 9: Group velocity *versus* axial force with $\eta = 0.5$ and $f = 6$ kHz.

4.4. Application to Beams with Different Boundary Conditions. The analysis model consists of a beam fixed at both ends as shown in Figure 14 and a beam fixed at one end and free at the other as shown in Figure 15, respectively. Both beams share the common dimensions of $L = 3\text{m}S = 2 \times 10^{-4}\text{m}^2 I_b = 2 \times 10^{-10}\text{m}^4$, material properties of $\rho = 2700\text{kg/m}^3$ and $E = 70\text{GPa}$, and the structural damping loss factor $\eta = 0.5$. Since the energy outflow at the fixed point is zero and the energy flow satisfies the equilibrium condition at the driving point, the energy intensity boundary conditions for the fixed-fixed beam is identical to those for the pinned-pinned beam. However, the impedance of fixed-fixed beam at the driving point is obtained by substituting equations (B.5) and (B.6) in Appendix B into equation (A.8) in Appendix A. For fixed-free beam, the subdomain ② is absent so that the coefficients C_{21}, C_{22} in equation (29) vanish, the following matrix equation is rewritten as

$$\begin{bmatrix} 1 & -1 \\ -P_f e^{-\lambda_f x_0} & P_f e^{\lambda_f x_0} \end{bmatrix} \begin{bmatrix} C_{11} \\ C_{12} \end{bmatrix} = \begin{bmatrix} 0 \\ \langle \pi_{\text{in}} \rangle \end{bmatrix}. \tag{30}$$

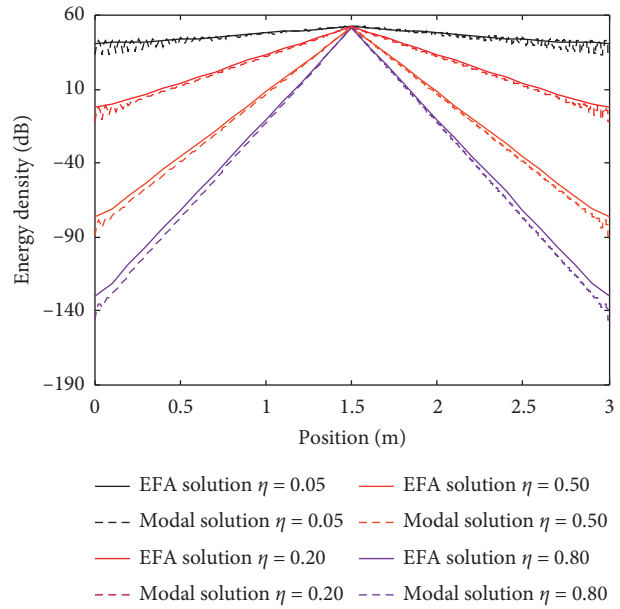

FIGURE 10: Energy density distribution of pinned-pinned beams with $N = 20$ kN, $F_0 = 1$ N, and $f = 6$ kHz when $\eta = 0.05$, 0.20, 0.50, 0.80.

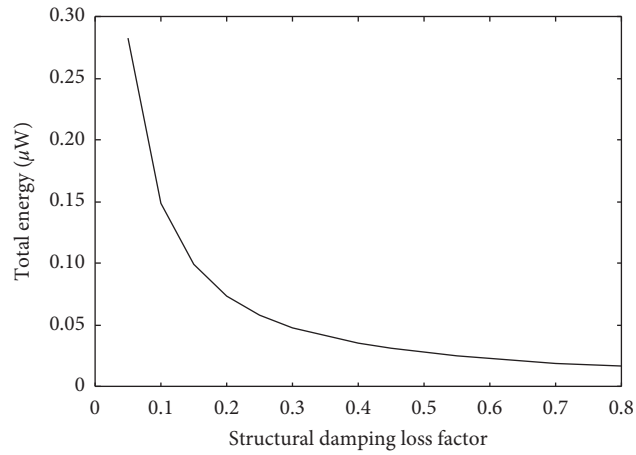

FIGURE 11: Total energy of pinned-pinned beams *versus* structural damping loss factor with $F_0 = 1$ N, $N = 20$ kN, and $f = 6$ kHz.

Similarly the impedance of fixed-free beam at driving point is determined by substituting the equation (B.8) and (B.9) in Appendix B into equation (A.8) in Appendix A. From equation (30), the energy density for the fixed-fixed beam can be evaluated.

Figure 14 shows a fixed-fixed beam with constant axial force. Figures 16 and 17 show the energy density distribution of fixed-fixed beams and fixed-free beams with $F_0 = 1$ N, $N = 20$ kN, and $\eta = 0.5$ when the analysis frequencies are 2 kHz, 4 kHz, 6 kHz, and 8 kHz, respectively. The developed EFA results coincide well with the overall trend of the exact solutions from modal analysis at each frequency. Similar to previous cases, the developed energy flow model gives more accurate result at high frequencies despite the exclusion of

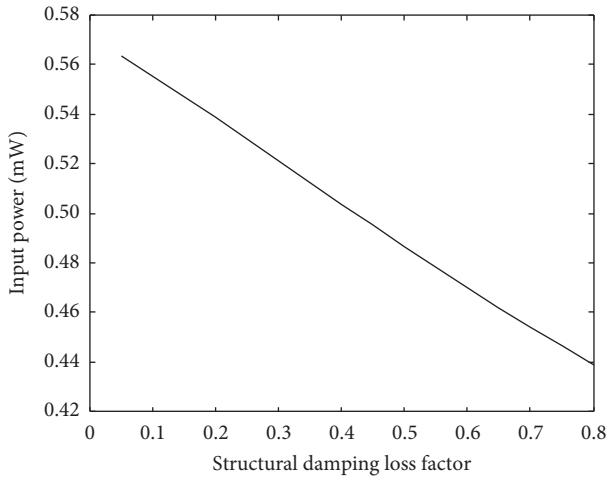

Figure 12: Input power of pinned-pinned beams *versus* structural damping loss factor with $F_0 = 1$ N, $N = 20$ kN and $f = 6$ kHz.

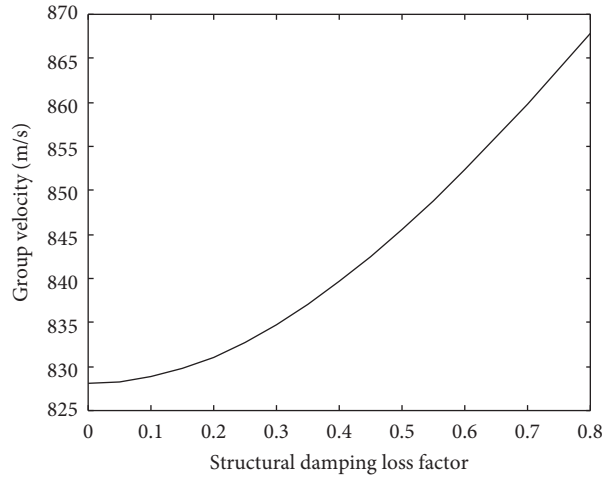

Figure 13: Group velocity *versus* structural damping loss factor with $N = 20$ kN and $f = 6$ kHz.

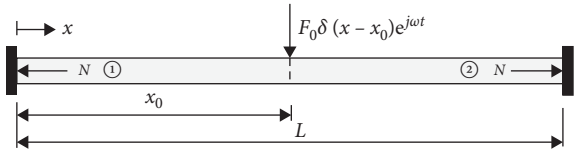

Figure 14: A fixed-fixed beam with constant axial force.

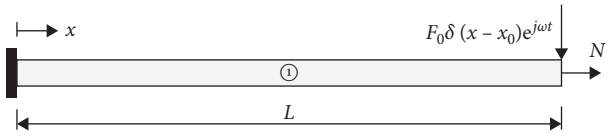

Figure 15: A fixed-free beam with constant axial force.

the evanescent wave. As a consequence, it is feasible to predict the vibrational energy density of beams with various boundary conditions in the high-frequency range by the proposed energy flow model.

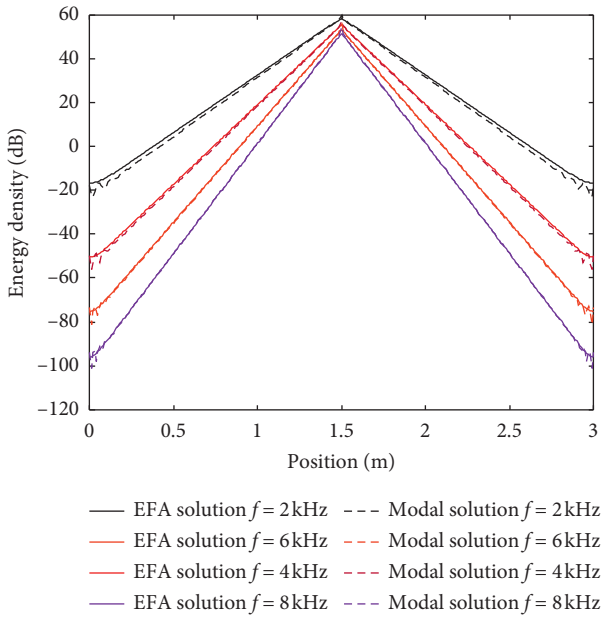

Figure 16: Energy density distribution of fixed-fixed beams with $F_0 = 1$ N, $N = 20$ kN, and $\eta = 0.5$ when $f = 2$, 4, 6, 8 kHz.

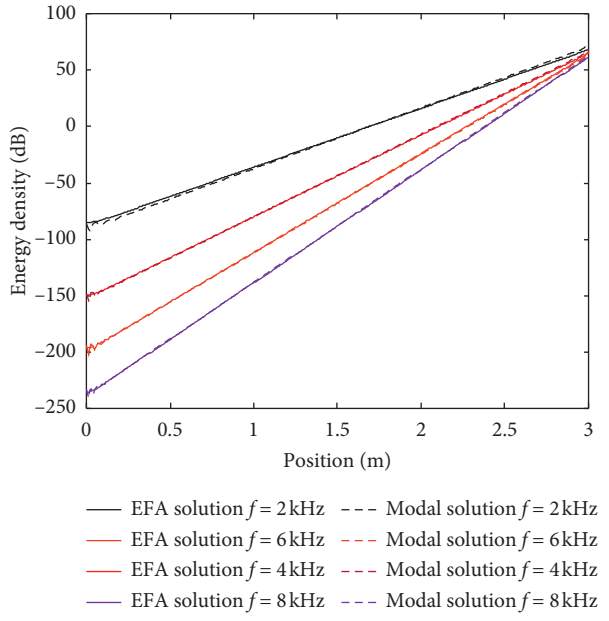

Figure 17: Energy density distribution of fixed-free beams with $F_0 = 1$ N, $N = 20$ kN, and $\eta = 0.5$ when $f = 2$, 4, 6, 8 kHz.

5. Conclusion

An energy flow model for a beam with axial force that includes high damping effect is established to evaluate the energy density in the high-frequency range. The wavenumber is expressed as the function of the damping loss factor and the axial force. Particularly, the energy transmission equation and the energy dissipation equation are derived from the wavenumber without approximation of its real and imaginary term. Then, the energy density governing

equation is obtained for the high damping beam with axial force.

To verify the developed energy flow model, numerical analyses are performed for the simply supported beam with various damping loss factor and axial force. The EFA solutions are greatly consistent with the modal solutions in all cases. Furthermore, it is found that both the high damping factor and large axial force can significantly alter the level of energy density as well as the distribution. Due to the resulting deceasing input power, the increasing damping loss factor makes the energy density decay more dramatically along axial position. However, that is the contrary case for the axial force. The proposed method is expected to be useful for the prediction of the high-frequency vibration of high damping structures with initial stress.

Appendix

A. Impedance and Exact Solution from Modal Analysis for High Damping Beams with Axial Force

When a high damping beam with axial force is excited at x_0 by a transverse harmonic force, the governing equation of motion can be expressed as

$$D_c\frac{\partial^4 w}{\partial x^4} - N_c\frac{\partial^2 w}{\partial x^2} + \rho S\frac{\partial^2 w}{\partial t^2} = F_0\delta(x - x_0)e^{j\omega t}. \tag{A.1}$$

The steady-state solution of equation (A.1) can be found by modal superposition as

$$w(x,t) = \sum_{i=1}^{\infty}\phi_i(x)q_i(t). \tag{A.2}$$

where $\phi_i(x)$ is the ith natural mode of the beam and $q_i(t)$ is the ith mode displacement.

By substituting equation (A.2) into the motion equation of the beam, equation (A.1), and using the orthogonality of natural modes, we obtain

$$K_i q_i(t) + M_i\frac{\mathrm{d}^2 q_i(t)}{\mathrm{d}t^2} = F_i, \tag{A.3}$$

where

$$F_i = \int_0^L F_0\delta(x - x_0)\phi_i(x)\mathrm{d}x, \tag{A.4}$$

represents the so-called "modal force" and

$$\begin{aligned} M_i &= \int_0^L \rho S\phi_i^2\mathrm{d}x, \\ K_i &= \omega_i^2(1 + j\eta)\int_0^L \rho S\phi_i^2\mathrm{d}x, \end{aligned} \tag{A.5}$$

are the so-called "modal mass" and "modal stiffness". The effect of structural damping is modeled by assuming a hysteretic damping model which introduces an additional complex term $(1 + j\eta)$ to modal stiffness. The natural frequency of the ith mode, ω_i, can be determined from the corresponding wavenumber in equation (2), which can be written as

$$k_i^2 = -\frac{N}{2D} + \sqrt{\left(\frac{N}{2D}\right)^2 + \frac{\rho S\omega_i^2}{D}}. \tag{A.6}$$

The forced vibration response of the beam can be expressed as the linear combination of the normal modes

$$w(x,t) = \sum_{i=1}^{\infty}\frac{F_0\cdot e^{j\omega t}}{M_i\left[\omega_i^2(1 + j\eta) - \omega^2\right]}\phi_i(x)\phi_i(x_0). \tag{A.7}$$

The impedance at the driving point of the finite beam with axial force can be obtained from its definition:

$$Z = \frac{F_0 e^{j\omega t}}{\dot{w}(x_0,t)} = \frac{-1}{\sum_{i=1}^{\infty}\omega\phi_i^2(x_0)/M_i\left[\omega_i^2(1 + j\eta) - \omega^2\right]}, \tag{A.8}$$

where $\dot{w}(x_0,t)$ is the velocity at driving point, which can be calculated as the time derivative of the displacement at $x = x_0$. Once the mode function is determined by the boundary condition, the impedance at driving point of the finite beam with axial force is derived from equation (A.8).

The time averaged energy density is given by

$$\langle e\rangle = \frac{1}{4}\left[\rho S\left(\frac{\partial w}{\partial t}\right)\left(\frac{\partial w}{\partial t}\right)^* + D\left(\frac{\partial^2 w}{\partial x^2}\right)\left(\frac{\partial^2 w}{\partial x^2}\right)^* + N\left(\frac{\partial w}{\partial x}\right)\left(\frac{\partial w}{\partial x}\right)^*\right]. \tag{A.9}$$

Substituting equation (A.7) into equation (A.9), the energy density can be obtained based on the modal solution.

B. Mode Shapes for High Damping Beams with Axial Force

B.1. Beam Pinned at Both Ends. The transverse displacement and the bending moment are zero at a simply supported end. Hence, the boundary conditions can be stated as

$$\begin{aligned} w(0) &= 0, \\ \frac{\partial^2 w(0)}{\partial x^2} &= 0, \\ w(L) &= 0, \\ \frac{\partial^2 w(L)}{\partial x^2} &= 0. \end{aligned} \tag{B.1}$$

The general solution of equation (A.1) is shown in equation (7), whereas the frequency equation with both simply supported ends is derived as

$$\sin k_i L = 0. \tag{B.2}$$

The vibration mode of the beam is given by

$$\phi_i(x) = \sin k_i x. \tag{B.3}$$

B.2. Beam Fixed at Both Ends. At a fixed end, the transverse displacement and the slope of the displacement are zero. Hence, the boundary conditions are given by

$$\begin{aligned} w(0) &= 0, \\ \frac{\partial w(0)}{\partial x} &= 0, \\ w(L) &= 0, \\ \frac{\partial w(L)}{\partial x} &= 0. \end{aligned} \tag{B.4}$$

By virtue of general solution in equation (7) and boundary conditions with both fixed ends, the frequency equation is obtained as

$$\cos k_i L \cosh k_i L - 1 = 0. \tag{B.5}$$

The vibration mode of the beam is expressed as

$$\begin{aligned} \phi_i(x) = &\left(\cos k_i x - \cosh k_i x\right) + \frac{\cos k_i L - \cosh k_i L}{\sin k_i L - \sinh k_i L} \\ &\cdot \left(\sin k_i x - \sinh k_i x\right). \end{aligned} \tag{B.6}$$

B.3. Beam Fixed at One End and Free at the Other. If the beam is fixed at $x = 0$ and free at $x = L$, the transverse deflection and its slope must be zero at $x = 0$ and the bending moment and shear force must be zero at $x = L$. Thus, the boundary conditions become

$$\begin{aligned} w(0) &= 0, \\ \frac{\partial w(0)}{\partial x} &= 0, \\ \frac{\partial^3 w(L)}{\partial x^3} &= 0, \\ \frac{\partial^2 w(L)}{\partial x^2} &= 0. \end{aligned} \tag{B.7}$$

According to the general solution in equation (7) and boundary conditions with one fixed end and the other free end, the frequency equation is derived as

$$\cos k_i L \cosh k_i L + 1 = 0. \tag{B.8}$$

The vibration mode of the beam is written as

$$\begin{aligned} \phi_i(x) = &\left(\cos k_i x - \cosh k_i x\right) + \frac{\cos k_i L + \cosh k_i L}{\sin k_i L + \sinh k_i L} \\ &\cdot \left(\sin k_i x - \sinh k_i x\right). \end{aligned} \tag{B.9}$$

Data Availability

The data used to support the finding of this study are available from the corresponding author upon request.

Conflicts of Interest

The authors declare that there no conflicts of interest.

Acknowledgments

The presented work was supported by National Natural Science Foundation of China (Grant no. 51505096) and Natural Science Foundation of Heilongjiang Province of China (Grant no. QC2016056).

References

[1] L. Bot, "Entropy in sound and vibration: towards a new paradigm," *Proceedings of the Royal Society A: Mathematical, Physical and Engineering Science*, vol. 473, no. 2197, pp. 1–9, 2017.

[2] A. Acri, "A literature review on energy flow analysis of vibrating structures," *ASRO Journal of Applied Mechanics*, vol. 1, no. 1, pp. 12–15, 2017.

[3] J. C. Wohlever and R. J. Bernhard, "Mechanical energy flow models of rods and beams," *Journal of Sound and Vibration*, vol. 153, no. 1, pp. 1–19, 1992.

[4] Z. Chen, Z. Yang, Y. Wang, and X. Wang, "A high-frequency shock response analysis method based on energy finite element method and virtual mode synthesis and simulation," *Acta Aeronautica et Astronautica Sinica*, vol. 39, no. 08, pp. 182–191, 2018.

[5] Z. Liu and J. Niu, "Vibrational energy flow model for functionally graded beams," *Composite Structures*, vol. 186, pp. 17–28, 2018.

[6] X. Kong, H. Chen, D. Zhu, and W. Zhang, "Study on the validity region of energy finite element analysis," *Journal of Sound and Vibration*, vol. 333, no. 9, pp. 2601–2616, 2014.

[7] A. Nokhbatolfoghahai, H. Navazi, Y. Ghobaad, and H. Haddadpour, "Experimental measurement of energy density of a vibrating beam," *Journal of Vibration and Control*, vol. 24, no. 24, pp. 5735–5746, 2018.

[8] H. M. Navazi, A. Nokhbatolfoghahaei, Y. Ghobad, and H. Haddadpour, "Experimental measurement of energy density in a vibrating plate and comparison with energy finite element analysis," *Journal of Sound and Vibration*, vol. 375, pp. 289–307, 2016.

[9] D. Zhu, H. Chen, X. Kong, and W. Zhang, "A hybrid finite element-energy finite element method for mid-frequency vibrations of built-up structures under multi-distributed loadings," *Journal of Sound & Vibration*, vol. 333, no. 22, pp. 5723–5745, 2014.

[10] M. Sadeghmanesh, H. Haddadpour, M. T. Abadi, and H. M. Navazi, "A method for selection of structural theories

for low to high frequency vibration analyses," *European Journal of Mechanics-A Solids*, vol. 75, pp. 27–40, 2019.

[11] W. Zhang, A. Wang, N. Vlahopoulos, and K. Wu, "A vibration analysis of stiffened plates under heavy fluid loading by an energy finite element analysis formulation," *Finite Elements in Analysis and Design*, vol. 41, no. 11-12, pp. 1056–1078, 2005.

[12] J.-B. Han, S.-Y. Hong, and J.-H. Song, "Energy flow model for thin plate considering fluid loading with mean flow," *Journal of Sound and Vibration*, vol. 331, no. 24, pp. 5326–5346, 2012.

[13] H.-W. Kwon, S.-Y. Hong, D.-K. Oh et al., "Experimental study on the energy flow analysis of underwater vibration for the reinforced cylindrical structure," *Journal of Mechanical Science and Technology*, vol. 28, no. 9, pp. 3405–3410, 2014.

[14] S. Wang and R. J. Bernhard, "Prediction of averaged energy for moderately damped systems with strong coupling," *Journal of Sound and Vibration*, vol. 319, no. 1-2, pp. 426–444, 2009.

[15] V. S. Pereira and J. M. C. Dos Santos, "Coupled plate energy models at mid- and high-frequency vibrations," *Computers & Structures*, vol. 134, pp. 48–61, 2014.

[16] H.-W. Kwon, S.-Y. Hong, and J.-H. Song, "Vibrational energy flow analysis of coupled cylindrical thin shell structures," *Journal of Mechanical Science and Technology*, vol. 30, no. 9, pp. 4049–4062, 2016.

[17] Y.-H. Park and S.-Y. Hong, "Hybrid power flow analysis using coupling loss factor of SEA for low-damping system-part I: formulation of 1-D and 2-D cases," *Journal of Sound and Vibration*, vol. 299, no. 3, pp. 484–503, 2007.

[18] Z. Liu, J. Niu, and X. Gao, "An improved approach for analysis of coupled structures in Energy Finite Element Analysis using the coupling loss factor," *Computers & Structures*, vol. 210, pp. 69–86, 2018.

[19] H.-W. Kwon, S.-Y. Hong, and J.-H. Song, "Energy flow models for underwater radiation noise prediction in medium-to-high-frequency ranges," *Proceedings of the Institution of Mechanical Engineers, Part M: Journal of Engineering for the Maritime Environment*, vol. 230, no. 2, pp. 404–416, 2016.

[20] X. Zheng, W. Dai, Y. Qiu, and Z. Hao, "Prediction and energy contribution analysis of interior noise in a high-speed train based on modified energy finite element analysis," *Mechanical Systems and Signal Processing*, vol. 126, pp. 439–457, 2019.

[21] W. Zhang, H. Chen, D. Zhu, and X. Kong, "The thermal effects on high-frequency vibration of beams using energy flow analysis," *Journal of Sound and Vibration*, vol. 333, no. 9, pp. 2588–2600, 2014.

[22] W. Di, X. Miaoxia, and L. Yueming, "High-frequency dynamic analysis of plates in thermal environments based on energy finite element method," *Shock and Vibration*, vol. 2015, pp. 1–14, 2015.

[23] Z. Chen, Z. Yang, N. Guo, and G. Zhang, "An energy finite element method for high frequency vibration analysis of beams with axial force," *Applied Mathematical Modelling*, vol. 61, no. 5, pp. 521–539, 2018.

[24] P. M. Morse and K. U. Indard, *Theoretical Acoustics*, Princeton University Press, Princeton, NJ, USA, 1986.

[25] W. Weaver, S. P. Timoshenko, and D. H. Young, *Vibration Problems in Engineering*, John Wiley & Sons, Hoboken, NJ, USA, 1990.

[26] M. N. Ichchou, A. Le Bot, and L. Jezequel, "Energy models of one-dimensional, multi-propagative systems," *Journal of Sound and Vibration*, vol. 201, no. 5, pp. 535–554, 1997.

[27] Y. Lase, M. N. Ichchou, and L. Jezequel, "Energy flow analysis of bars and beams: theoretical formulations," *Journal of Sound and Vibration*, vol. 192, no. 1, pp. 281–305, 1996.

[28] D. J. Nefske and S. H. Sung, "Power flow finite element analysis of dynamic systems: basic theory and application to beams," *Journal of Vibration and Acoustics*, vol. 111, no. 1, pp. 94–100, 1989.